Environ Monit Assess (2022) 194:762
https://doi.org/10.1007/s10661-022-10444-7

Changes in air quality over different land covers associated with COVID-19 in Turkey aided by GEE

Dilek Kucuk Matci · Gordana Kaplan · Ugur Avdan

Received: 7 February 2022 / Accepted: 30 August 2022 / Published online: 10 September 2022

Abstract With the increased urbanization, the rise of the manufacturing industry, and the use of fossil fuels, poor air quality is one of the most serious and pressing problems worldwide. The COVID-19 outbreak prompted absolute lockdowns in the majority of countries throughout the world, posing new research questions. The study's goals were to analyze air and temperature parameters in Turkey across various land cover classes and to investigate the correlation between air and temperature. For that purpose, remote sensing data from MODIS and Sentinel-5P TROPOMI were used from 2019 to 2021 over Turkey. A large amount of data was processed and analyzed in Google Earth Engine (GEE). Results showed a significant decrease in NO_2 in urban areas. The findings can be used in long-term strategies for lowering global air pollution. Future research should look at similar investigations in various study sites and evaluate changes in air metrics over additional classes.

Keywords Remote sensing · Air quality · MODIS · Land cover · Turkey · GEE

Introduction

Poor air quality is one of the most serious and pressing problems in emerging nations, and it is mainly caused by increasing urbanization, the development of the manufacturing industry, and the use of fossil fuels in industrial and residential activities (Angelevska et al., 2021; Ghasempour et al., 2021). Carbon monoxide (CO), nitrogen dioxide (NO_2), ozone (O_3), sulfur dioxide (SO_2), and particulate matter (including PM_{10} and $PM_{2.5}$) emissions from human and natural sources have a substantial influence on individual health and well-being (Gopalakrishnan et al., 2018). With more than half of the world's population living in cities, the impact of air pollution on public health must be addressed. Energy consumption, industrial emissions, and automobile traffic all rise when cities develop in population and size, all of which can have a negative impact on air quality (Kahyaoğlu-Koračin et al., 2009). Conversion of forests, grasslands, and cropland to urban development, industrial complexes, and big commercial areas frequently results in increased emissions. Urban sprawl is the most severe example of this sort of growth, characterized by dispersed patterns of low-density development, which is frequently automobile-oriented (Superczynski & Christopher, 2011). Inevitably, air quality varies based on land cover and as the environment changes. The air quality impacts of different land covers have been researched in a number of studies. Thus, the air quality impacts of grasslands and shrublands have been investigated in the USA (Gopalakrishnan et al., 2018) for the primary purpose of estimating the pollution removal capacity of canopy cover on a national level. Spatial interpolation of air pollution measurements was done, and the land cover was considered (Janssen et al., 2008). As a land use

D. K. Matci · G. Kaplan (✉) · U. Avdan
Institute of Earth and Space Sciences, Eskisehir Technical University, Eskisehir, Türkiye
e-mail: kaplangorde@gmail.com

pattern, CORINE land cover maps were employed, which were divided into numerous types. In situ data, however, were utilized in the previous research. For credible decision-making to mitigate the impact of air pollution, continuous and reliable air quality monitoring is essential.

Remote sensing techniques and geo-information systems provide complementary information for unreachable areas and for acquiring information about the Earth, such as land and sea surface temperature (Khorrami et al., 2019; Nacef et al., 2016), vegetation cover (Gao et al., 2020), and air quality (Kaplan & Avdan, 2020a, 2020b), and even predict and evaluate natural disasters (Çömert et al., 2019). Long-term spatiotemporal air quality monitoring [11, 12] at diverse scales is thus conceivable using satellite-based remote sensing methods (Kaplan & Avdan, 2020a, 2020b). Satellite observation for air quality has been used for over four decades, starting with the launch of the Total Ozone Monitoring Instrument (TOMS) in 1978, GOME in 1995 (Burrows et al., 1999), Ozone Monitoring Instrument (OMI) in 2004, and Sentinel-5 Precursor Tropospheric Monitoring Instrument (Sentinel-5P TROPOMI) in 2017, and satellite instruments are designed to observe several gases in the Earth's stratosphere and troposphere. For example, Jabeen and Khokhar (2019) used low-spatial resolution OMI satellite data for monitoring the atmospheric burdens of SO_2 over Pakistan over a time period of 2005–2016, while Hou et al. (2019) used OMI satellite data for investigating the temporal and spatial dynamics of NO_2 over China. Oner and Kaynak (2016) evaluated the NO_x emissions from available inventories using satellite NO_2 retrievals from OMI over Turkey. TROPOMI, compared to other air-quality monitoring satellite instruments, has a reasonably high spatial resolution, which is required for air quality applications (Abida et al., 2016). Since the launch of Sentinel-5P, several researchers have used the TROPOMI in various air monitoring studies. Thus, Kaplan et al. (2019) used TROPOMI data for monitoring the NO_2 over Turkey and correlate it with population density, Theys et al. (2019) investigated volcanic SO_2, and Borsdorff et al. (2018) presented the first results of measuring CO with TROPOMI over China. Statistical analyses of the global comparison between TROPOMI and ground-based measurements show a small percentage difference (Garane et al., 2019).

With the availability of data from TROPOMI, and notably the COVID-19 epidemic, researchers began to explore the effect of the new situation globally, and the number of air quality and air pollution studies using remote sensing data rapidly increased (Fig. 1). The first Copernicus mission and the most current satellite-based sensor for air quality monitoring, Sentinel-5P's TROPOMI, launched on October 13, 2017, is the first Copernicus mission and the most recent satellite-based sensor for air quality monitoring. It has been providing high spatiotemporal resolution data for monitoring air quality indicators, including the Absorbing Aerosol Index (AAI or UVAI), O_3, CO, NO_2, SO_2, CH_4, cloud characteristics, and formaldehyde (HCHO). Impacts on people's daily activities and migratory patterns have

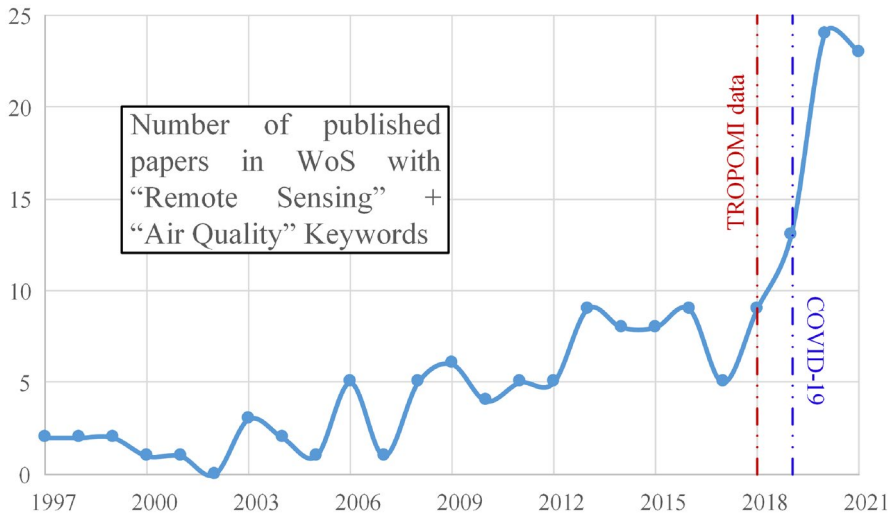

Fig. 1 Number of papers published in the Web of Science with "Remote Sensing" and "Air Quality" author keywords

resulted in many environmental changes. Some of the first data on this topic were released for Turkey, where half reduced NO_2 levels in major cities such as Istanbul, Bursa, Kocaeli, and Yalova during the first month of the COVID-19 lockdown (15 March–15 April) (Kaplan & Avdan, 2020a, 2020b). Similar results for Turkey were also published in a wider span of time (Ghasempour et al., 2021). On the same topic, a number of studies have been undertaken across the world (Berman & Ebisu, 2020; Elshorbany et al., 2021; Fan et al., 2020; Ghahremanloo et al., 2021; Metya et al., 2020; Qiu et al., 2021; Tobías et al., 2020). The positive effects of people's daily migration restrictions are evident in most of the studies. However, none of the research cited has looked at the influence of various land cover types. Until recently, the majority of studies concentrated on land cover changes and their impact on the environment (Kafy et al., 2020; Tadese et al., 2020).

The pandemic outbreak prompted absolute lockdowns in the majority of countries throughout the world, posing new research issues. This is the first time in Earth's history that we have data from remote sensing sensors before, during, and after a pandemic, and for the first time, this data can be utilized to monitor air quality. Because of recent developments in the remote sensing field, such as the Google Earth Engine (GEE), this massive amount of data can only be analyzed in a short length of time. GEE is a cloud-based geospatial processing application that allows users to conduct analysis fast. All of the data in GEE has an open-source component. These data are from the last 40 years and may be utilized to undertake global data mining. Turkey has been selected as a study area, and the study objectives are as follows: (i) evaluating the air and temperature parameters over different land cover classes; and (ii) evaluating the results regarding COVID-19 restrictions.

Materials and methods

Study area

Turkey is a transcontinental country centered on the Anatolian peninsula in Western Asia, with a minor component in Southeast Europe's East Thrace. Turkey is administratively organized into 81 provinces under this unified framework. Turkey is split into seven regions and twenty-one subregions for topographical, demographic, and economic reasons. Turkey's Aegean Sea and Mediterranean Sea coasts have a hot-summer Mediterranean climate, with hot, dry summers and warm-to-chilly, rainy winters. Turkey's Black Sea coast has a moderate Oceanic climate with warm, rainy summers and mild to cold, wet winters. Warm-to-hot, relatively dry summers and cool-to-cold, rainy winters characterize the coastal parts of Turkey surrounding the Sea of Marmara (including Istanbul), which connects the Aegean Sea with the Black Sea. Covering 783,356 km^2, Turkey is considered a large country. In terms of land cover, more than 40 percent of the country are covered with agricultural areas.

In contrast, forests cover 15 percent of the total land area, primarily coastal and mountainous (Ustaoglu & Aydınoglu, 2019). Grasslands also cover a significant part of the country. Taking this into consideration, Turkey's land cover can be divided into eight main classes: Forest, Shrubs, Grassland, Urban, Cropland, Barren land, Water, and Wetlands.

Regarding air quality, Turkey's air pollution is the most dangerous of the country's environmental problems, with levels across the country exceeding World Health Organization (WHO) recommendations (Organization, 2021; Varol et al., 2021). Each year, over 30,000 individuals die from air pollution-related diseases, accounting for more than 8% of all fatalities in the country. Road transport and coal are major pollutants in Turkish cities, but vehicle density is the most crucial factor impacting air pollution levels. COVID-19 restrictions reduced air pollution in major cities in early 2020.

Materials

For the study, we use datasets from three different sensors. Mainly MODIS, Sentinel-5p TROPOMI, and NCEP/NCAR. The land cover classes were determined using the MODIS MCD12Q1 V6 product. This data with a spatial resolution of 500 m presents global land cover data for 2001–2019. In the study, the land cover classes from 2019 were used. This product was obtained by classifying MODIS Terra and Aqua data using the supervised classification method. Data provides different layers: land cover type 1–5, land cover property 1–3, land cover property assessment 1–3, land cover quality control (QC), and a land water mask. Land cover type 1 data was used in this study (Sulla-Menashe & Friedl, 2018). For the study, the

main classes of the dataset were combined into eight classes (Forest, Shrubs, Grassland, Urban, Cropland, Barren land, Water, and Wetlands; Fig. 2).

SO_2, CO, NO_2, CH_4, and O_3 values, whose changes were examined in the study, were obtained using the datasets provided by the Sentinel-5P TROPOMI sensor. TROPOMI measures surface UV radiation and concentrations of various atmospheric components, including O_3, NO_2, SO_2, CO, CH_4, CH_2O, and aerosol. TROPOMI's four individual spectrometers measure the ultraviolet (UV), UV–visible (UV–VIS), near-infrared (NIR), and short-wavelength infrared (SWIR) spectral bands (ESA, 2020). Mean monthly TROPOMI data from January 2019 to October 2021 were used (Fig. 3).

The temperature values examined in the study were taken from NCEP and NCAR data. The NCEP/NCAR Reanalysis Project is a joint project between the National Centers for Environmental Prediction (NCEP) and the National Center for Atmospheric Research (NCAR), and the data were acquired for the same period as for TROPOMI. This project aims to produce new atmospheric analyses using historical data and analyses of the current atmospheric situation. The NCEP/NCAR Reanalysis-1 Project uses a state-of-the-art analysis/prediction system to perform data assimilation using historical data from 1948 to the present. The data has a temporal resolution of 6 h and a spatial resolution of 2.5 degrees (Kalnay et al., 1996).

Methodology

In order to investigate the air quality over different land cover classes over Turkey, several datasets have been selected in this paper. Data processing, data extraction, and data visualization were done in GEE. First, MODIS land cover data has been used to consider the spatial resolution of the air parameters data (Sentinel-5P, TROPOMI). The MODIS dataset was combined into eight land cover classes, Forest, Shrubs, Grassland, Urban, Cropland, Barren land, Water, and Wetlands. These are the main eight classes over the selected study area. The polygons of the selected land cover classes were used to extract the air parameters from the Sentinel-5P TROPOMI sensor. While the MODIS data were used for a single year (2019), the TROPOMI data were used for three periods, 2019, 2020, and January–November 2021. Thus, mean monthly values of SO_2, CO, NO_2, CH_4, and O_3 data were obtained for every class separately. In addition, NCEP/NCAR data were obtained for the temperature variations in the investigated period. The obtained data were analyzed using statistical analysis. First, the air parameters were analyzed separately for every class. In the second stage, the relationship between the investigated parameters was analyzed. A detailed flowchart of the applied methodology is given in Fig. 4.

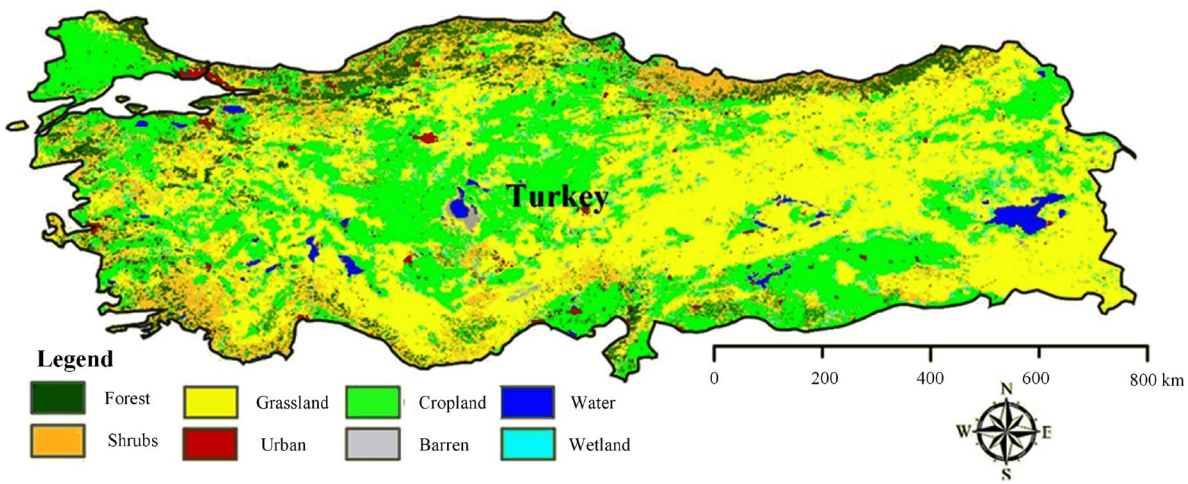

Fig. 2 MODIS land cover

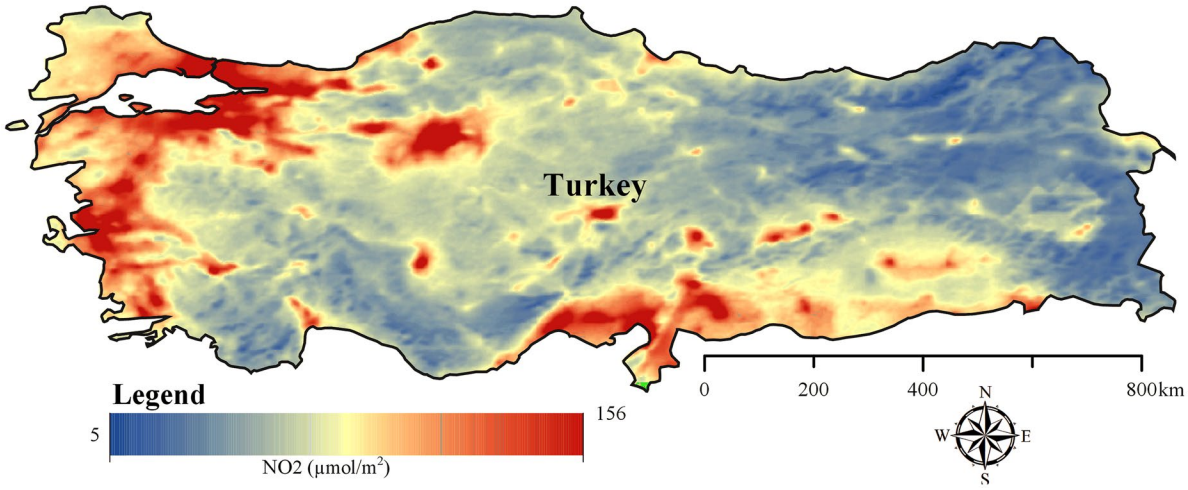

Fig. 3 Mean NO_2 over Turkey in the investigated period

Results and discussion

Since 2018, the TROPOMI sensor has provided significant high-resolution data about air quality and pollution. Since then, the Earth has been through a pandemic that positively has affected the air quality in many areas worldwide. Within the study area, available 1-year data before and after the pandemic opens potential research hypotheses over the studied period. The results of this study are presented in Figs. 5–8 and Table 1. First, the single parameter data will be presented, and then the relationship between the parameters will be discussed.

Over the time investigated, the NO_2 differed the most within the study area. The minimum NO_2 for all classes was recorded in 2020. The Urban class noticed the biggest difference: the minimum NO_2 value for 2019 and 2021 was 89 and 93 µm/mol^2, respectively, while for 2020 it was 80 um/mol^2. It should also be noted, that while the minimum values for 2019 were in August, and for 2021 in April, the minimum value for 2020 was in May, one of the strictest months in terms of quarantine in Turkey. In May 2019 and 2021, the NO_2 value was the same for both years, 95 um/mol^2. Also, while in March there is a significant high value in the year 2019 (102 umol/m^2), and 105 for 2021, in 2020 the NO_2 value is 86 um/mol^2, which overlaps with the quarantine period in Turkey. For the other classes, also the minimum value is recorded in 2020. In comparison to 2020, the minimum NO_2 values are 4–7% higher in 2019 and 2020. Similar are the maximum values; the highest values were recorded in 2021 with small differences compared to 2019. Furthermore, the differences between the highest values between 2019 and 2021 and 2020 range from 6 to 7%. The results for NO_2 changes in the investigated period are given in Fig. 5. Figure 5 shows that compared with 2019 and 2021, the NO_2 values are lower in the COVID-19 strict precautions period. For instance, for the other classes other than Urban, the NO_2 in May 2019 varies from 76 to 90 um/mol^2, similar in May 2021 which varies from 75 to 89 umol/m^2, while in 2020 for the same period, the values vary from 66 to 71 umol/m^2. Visualization of the NO_2 differences is shown in Fig. 6.

The CO values over different classes are shown in Fig. 7. While there is no significant difference between the investigated years, there is a difference in the classes. Also, the seasonal variations of CO over the different classes can be seen. While the CO is low in the summer season, the maximum values can be noticed in the cold seasons. Thus, the maximum CO values can be noticed in the Urban class in every month over the 3 years. There is a significant lowering in the CO values at the start of the strict measurements in Turkey due to the pandemic, but similar movements are noticed in the previous and the year after. After the Urban class, Wetlands have the highest CO values in all investigated months, followed by Forest and Cropland. The lower CO values are noticed in the Grassland and Barren

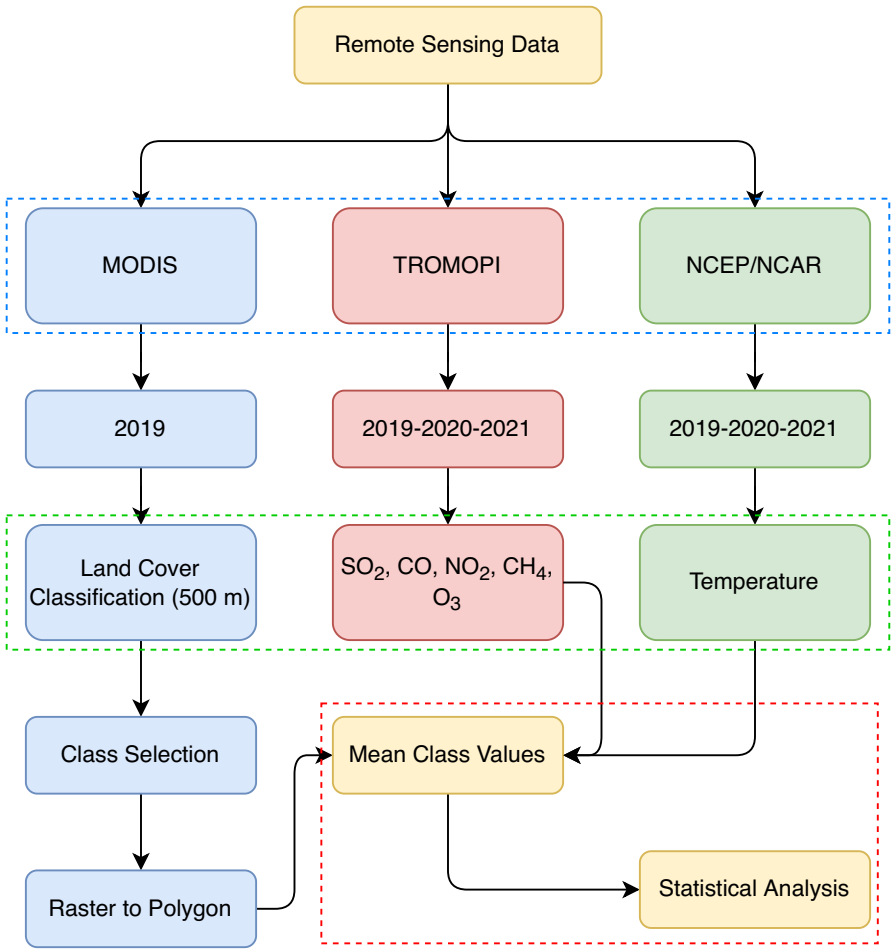

Fig. 4 Flowchart of the applied methodology

land classes (Fig. 7). For the CH_4 values, the highest value can be noticed in the Shrubs class, followed by Cropland, Barren land, and Urban areas. The lowest values are recorded in the Forest class. The results for the CH_4 are presented in Fig. 8. Here, the highest values can be noticed in the Shrubs class. The values are similar for Urban, Barren land, and Cropland classes, and Forest showed the lowest CH_4 values.

The SO_2 values were similar for all classes. Thus, visualization was not possible. In the investigated

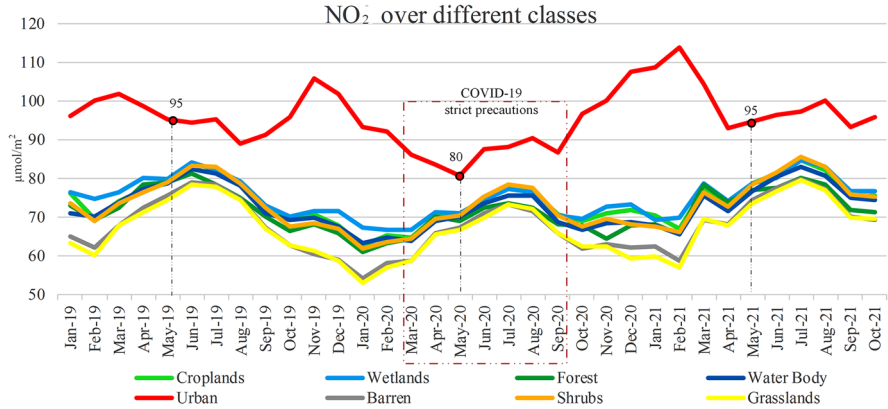

Fig. 5 NO_2 over different land cover classes with accent on the COVID-19 strict precaution period in Tukey

Table 1 Correlation between various air quality parameters (significance level $\alpha < 0.05$)

SO_2—temperature											
2019–2021			2019			2020			2021		
Class	*R*	R^2	Class	*R*	R^2	Class	*R*	R^2	Class	*R*	R^2
Cropland	**−0.78**	**0.61**	Cropland	**−0.61**	**0.37**	Cropland	−0.88	0.78	Cropland	−0.85	0.72
Wetlands	−0.74	0.55	Wetlands	−0.53	0.29	Wetlands	−0.89	0.79	Wetlands	−0.85	0.72
Forest	−0.72	0.52	Forest	−0.53	0.28	Forest	−0.85	0.73	Forest	−0.83	0.70
Water	−0.73	0.53	Water	−0.57	0.33	Water	−0.89	0.80	Water	−0.82	0.67
Urban	−0.74	0.55	Urban	−0.55	0.30	Urban	−0.90	0.81	Urban	−0.81	0.66
Barren land	−0.69	0.48	Barren land	−0.56	0.31	**Barren land**	**−0.92**	**0.84**	Barren land	−0.83	0.68
Shrubs	−0.71	0.50	Shrubs	−0.60	0.36	Shrubs	−0.81	0.66	Shrubs	−0.75	0.56
Grassland	−0.74	0.55	Grassland	−0.55	0.30	Grassland	−0.88	0.77	**Grassland**	**−0.87**	**0.76**
NO_2—temperature											
2019–2021			2019			2020			2021		
Class	*R*	R^2	Class	*R*	R^2	Class	*R*	R^2	Class	*R*	R^2
Cropland	0.66	0.44	Cropland	0.59	0.35	Cropland	0.79	0.62	Cropland	0.85	0.72
Wetlands	0.55	0.31	Wetlands	0.44	0.19	Wetlands	0.68	0.46	Wetlands	0.83	0.69
Forest	0.53	0.28	Forest	0.44	0.20	Forest	0.83	0.70	Forest	0.62	0.39
Water	0.69	0.48	Water	0.67	0.45	Water	0.79	0.63	Water	0.87	0.76
Urban	***−0.44***	***0.20***	***Urban***	***−0.66***	***0.44***	***Urban***	***−0.37***	***0.14***	***Urban***	***−0.65***	***0.42***
Barren land	0.77	0.59	Barren land	0.72	0.52	Barren land	0.86	0.73	Barren land	0.90	0.82
Shrubs	0.79	0.63	**Shrubs**	**0.74**	**0.55**	**Shrubs**	**0.86**	**0.74**	**Shrubs**	**0.92**	**0.84**
Grassland	**0.80**	**0.64**	Grassland	0.42	0.17	Grassland	0.81	0.65	Grassland	0.75	0.57
O_3—CH_4											
2019–2021			2019			2020			2021		
Class	*R*	R^2	Class	*R*	R^2	Class	*R*	R^2	Class	*R*	R^2
Cropland	−0.66	0.44	Cropland	−0.85	0.72	Cropland	−0.86	0.74	Cropland	−0.86	0.73
Wetlands	−0.66	0.43	**Wetlands**	**−0.89**	**0.78**	Wetlands	−0.93	0.86	Wetlands	−0.86	0.73
Forest	−0.53	0.28	Forest	−0.76	0.58	**Forest**	**−0.93**	**0.87**	Forest	−0.79	0.63
Water	−0.50	0.25	Water	−0.44	0.19	Water	−0.62	0.38	Water	−0.70	0.49
Urban	−0.62	0.39	Urban	−0.85	0.73	Urban	−0.89	0.79	Urban	−0.82	0.68
Barren land	**−0.73**	**0.53**	Barren land	−0.87	0.75	Barren land	−0.85	0.72	Barren land	−0.85	0.72
Shrubs	−0.69	0.48	Shrubs	−0.84	0.70	Shrubs	−0.82	0.67	**Shrubs**	**−0.88**	**0.78**
Grassland	−0.71	0.50	Grassland	−0.82	0.67	Grassland	−0.90	0.82	Grassland	−0.84	0.71

R Correlation coefficient, *R2* coefficient of determination

34 months, the highest SO_2 (mmol/m^2) values were recorded in December 2019, over the Barren land class. Overall, it can be noticed that the SO_2 values are highest during the autumn and winter months (October–February). The values were significantly lower from October 2020 to April 2021 compared to the previous year. While in the 2019–2020 season, the values were 1130–1435 mmol/m^2; for the 2020–2021 season, the values were 290–790 mmol/m^2. The highest values are different for all classes; for instance, the highest value in November 2020 was recorded over the Forest class, and in January 2021, over the Urban class. Although the O_3 values were similar, the values in 2020 were slightly lower compared to 2019 and 2020 for all classes. The temperature data did not show any difference between the investigated years. Shrubs and Urban areas were the hottest in the summer months, while in the cold months, the highest temperatures were recorded in the Forest areas, followed by Urban areas. The coldest class during all period was Barren land's class.

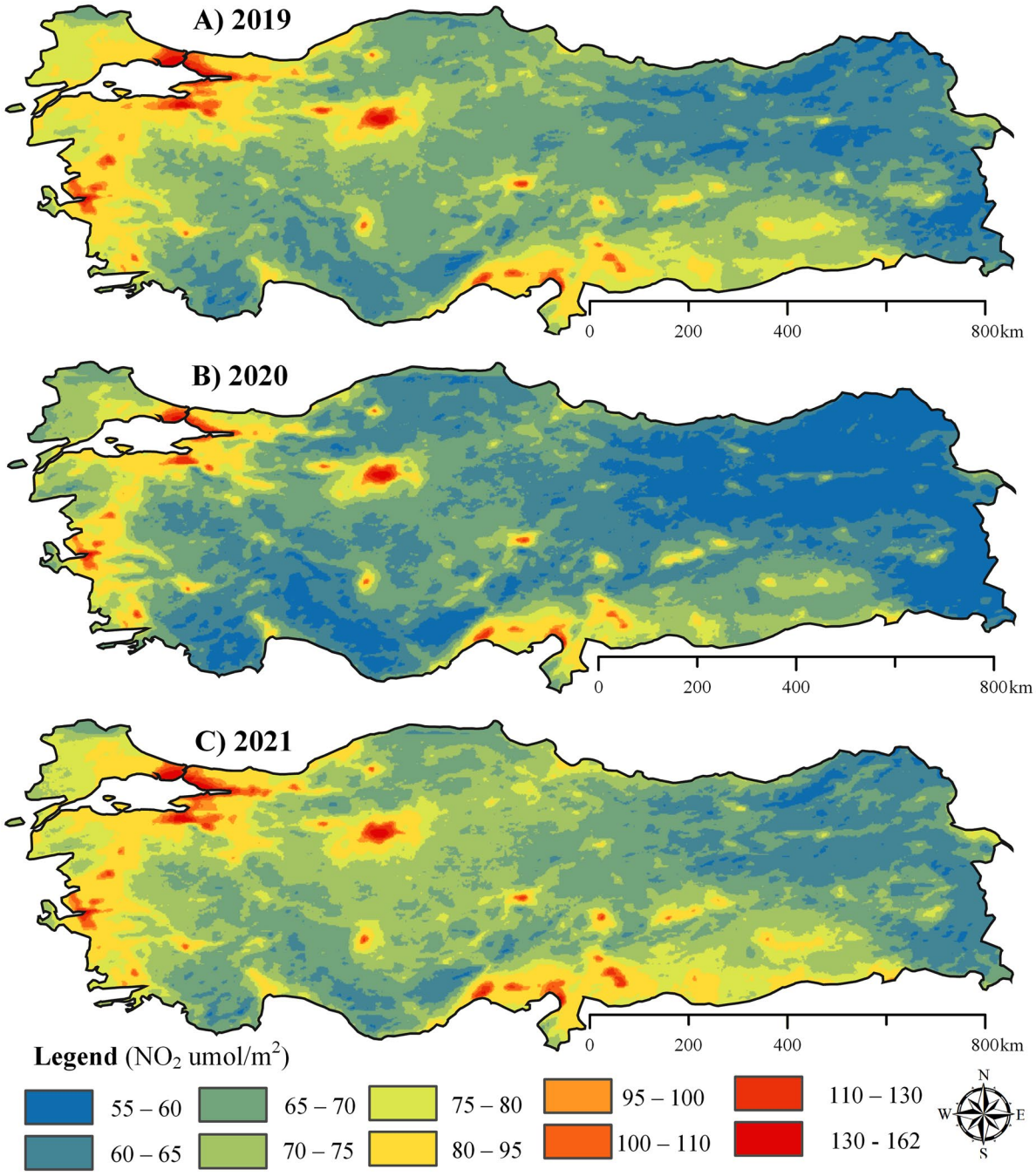

Fig. 6 Mean NO_2 values over Turkey for **A** 2019; **B** 2020; **C** 2021

The relationship between the parameters was investigated in four different periods, overall period and for the three years separately. In Table 1 are presented the values that were considered as significant ($R > 0.5$; significance level $\alpha < 0.05$). There was a significant relation between SO_2 and temperature, NO_2 and temperature, and O_3 and CH_4.

A significant negative relation has been noticed between SO_2 and temperature data. In 2019–2021, the highest relation was in the Cropland class

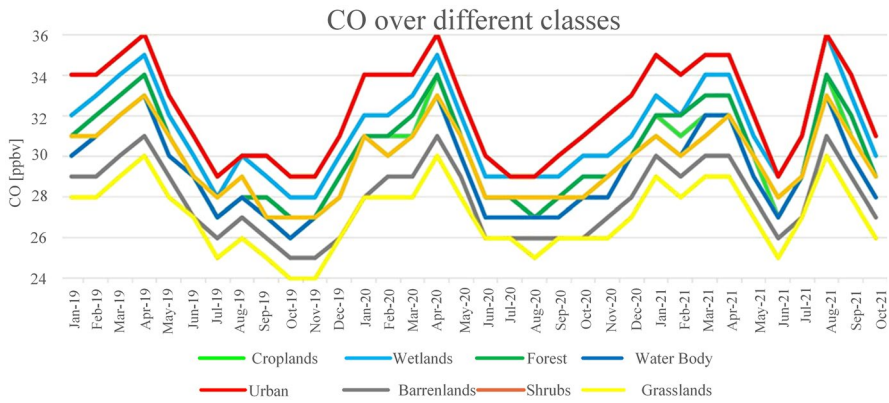

Fig. 7 CO over different land cover classes in Turkey

($R = -0.78$), and the lowest was over the Barren land class ($R = -0.69$). The relation was lowest in 2019 for all classes, highest for 2020, and slightly lower in 2021 than in 2020. A strong relation was noticed in 2020 in the Urban and Barren land classes ($R > 0.90$). Overall, for all classes and all months, the R^2 between SO_2 and temperature was 0.77 (Fig. 9). While there was a negative correlation between NO_2 and temperature data for the Urban class, for the other classes, the correlation was positive. For the positively correlated classes, the values were rising every year. Thus, while the R for the Cropland class in 2019 was 0.59, for 2020 and 2021, it was 0.79 and 0.85, respectively. While the results were similar for the other classes, for the Urban class, the correlation was -0.66 and -0.65 for 2019 and 2021, while for 2020, the correlation was significantly lower with $R = 0.37$. The correlation between O_3 and CH_4 was negative and stable for the investigated years.

In comparison with similar studies in the literature, the results are supported by the findings of several investigations. For example, a study conducted in China in 2015 examined the relationship between air pollutants and meteorological data in three big megacities. The results showed that as the temperature decreases, the pollutant rates increase (Zhang et al., 2015). A similar result was obtained in a study conducted in Erzurum. As a result of the study, it was determined that the CO and NO_x values decreased with the increase in temperature (Ocak & Turalioglu,

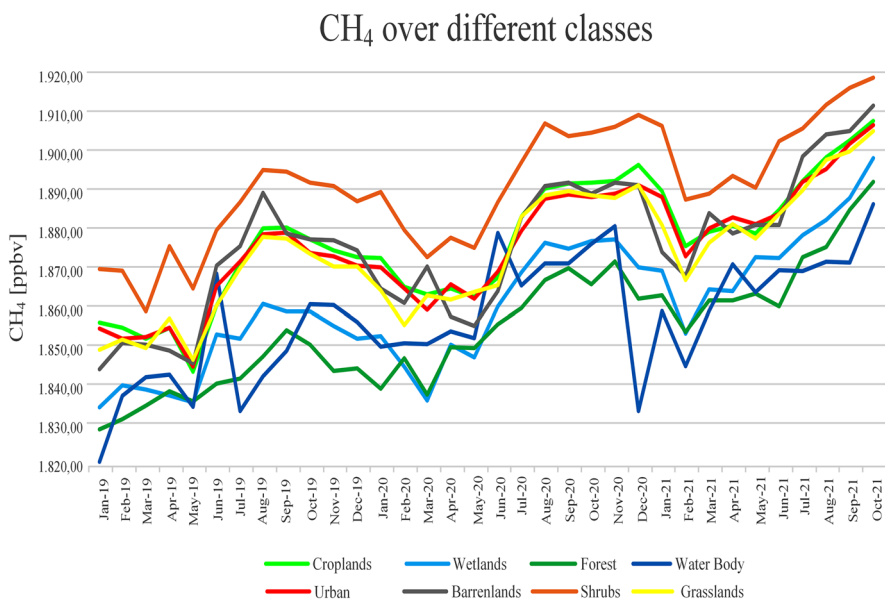

Fig. 8 CH_4 over different land cover classes in Turkey

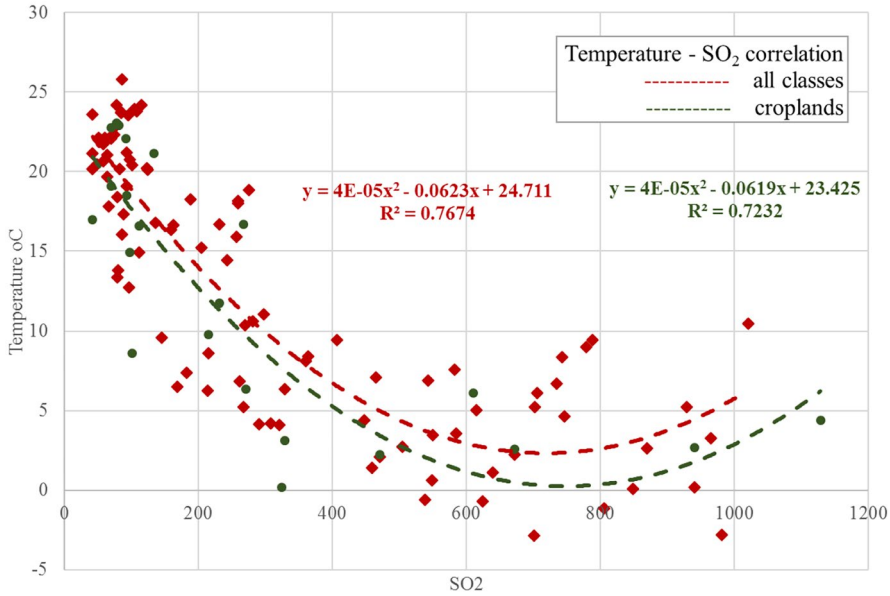

Fig. 9 Correlation between SO_2 and temperature for all classes (red) and croplands (green)

2008). In a study examining the number of patients affected by NO_2 with air temperature and other climatic parameters, it was stated that the highest NO_2 concentration was measured in autumn and winter, probably due to the increased use of motor vehicles and their exhaust gases (Pintarić et al., 2012).

The findings obtained in terms of the effect of the COVID-19 pandemic on air pollution are also similar to various studies. For example, the first evaluation of NO_2 over Turkey before and during the first lockdown period (15 March–15 April 2019–2020) (Kaplan & Avdan, 2020a, b) showed a significant lowering of NO_2 over the big cities in Turkey. The results of the broader study (January–September 2019, 2020) (Ghasempour et al., 2021) showed a lowering in the NO_2 between March and April. However, the mentioned study was performed with mean values over all of Turkey. The results of this study present the difference in the investigated land covers. In addition, many studies conducted worldwide (Alqasemi et al., 2021; Berman & Ebisu, 2020; Elshorbany et al., 2021; Ghahremanloo et al., 2021; Metya et al., 2020; Qiu et al., 2021) about the impact of the changes in peoples life's prompted by the COVID-19 pandemic revealed mainly positive environmental effects. In fact, the statement by Ghasempour et al. (2021) that the positive environmental effects of COVID-19 will not last a long time is confirmed by our study. Our investigation showed that the air quality parameters values in 2021 were back as the values in 2019.

Conclusion

The pandemic threat prompted complete lockdowns in most countries worldwide, posing new research questions. In this study, we used air quality data from the Sentinel-5P TROPOMI sensor to investigate differences in air quality and pollution across different land cover categories. The study's goals were to analyze air and temperature parameters in Turkey across various land cover classes and to look into the link between air and temperature parameters in general and across distinct land cover classes. The results show that NO_2 experienced severe changes in the Urban class, especially during the strict COVID-19 restriction over the study area. The results also show the seasonal variations of the investigated parameters over the different classes. The seasonal variations are most obvious in the CO values. Although NO_2 also tends to show seasonal variations, the influence of the COVID-19 lockdown is clear, as the values are significantly lower in the strictest pandemic precautions. The resolution of the used data limits the study as the land cover's accuracy is limited, which may lead to mixed pixels as small land cover classes that may fall within other larger classes. Even though the TROPOMI data are not as accurate as in situ data, with the satellite imagery, we have full coverage over the study area and are limited by the air quality data's spatial resolution.

The findings are crucial because they show the dynamics of air parameters before, during, and after

the COVID-19 epidemic. The findings might aid in developing new, long-term strategies for reducing air pollution throughout the planet. Similar investigations across other research regions and variations in different air characteristics over additional classes are proposed for future studies.

Author contribution Conceptualization: D. K. M., G. K., U. A. Data curation: D. K. M. Formal analysis: D. K. M., G. K. Investigation, methodology: D. K. M., G. K., U. A. Project administration: G. K. Supervision: U. A. Validation: D. K. M., G. K., U. A. Visualization: G. K. Writing—original draft: D. K. M., G. K. Writing—review and editing: D. K. M., G. K., U. A.

Funding This study was supported by Eskisehir Technical University Scientific Research Projects Commission under grant no: 21GAP064, Project: "MMARS—*M*apping and *M*onitoring *A*ir Quality and Air Pollution in Turkey Using *R*emote *S*ensing Data and Geo-Information Systems."

Data availability No available data.

Declarations

Conflict of interests The authors declare no conflict of interests.

References

Abida, R., El Amraoui, L., Ricaud, P., Lahoz, W., Eskes, H., Segers, A., Curier, L., de Haan, J., Nijhuis, A., & Schuettemeyer, D. (2016). Impact of spaceborne carbon monoxide observations from the S-5P platform on tropospheric composition analyses and forecasts. *Atmospheric Chemistry and Physics, 2016*(2), 1–1.

Alqasemi, A. S., Hereher, M. E., Kaplan, G., Al-Quraishi, A. M. F., & Saibi, H. (2021). Impact of COVID-19 lockdown upon the air quality and surface urban heat island intensity over the United Arab Emirates. *Science of the Total Environment, 767*, 144330.

Angelevska, B., Atanasova, V., & Andreevski, I. (2021). Urban air quality guidance based on measures categorization in road transport. *Civil Engineering Journal, 7*(2), 253–267.

Berman, J. D., & Ebisu, K. (2020). Changes in US air pollution during the COVID-19 pandemic. *Science of the Total Environment, 739*, 139864.

Borsdorff, T., Aan de Brugh, J., Hu, H., Aben, I., Hasekamp, O., & Landgraf, J. (2018). Measuring carbon monoxide with TROPOMI: First results and a comparison with ECMWF-IFS analysis data. *Geophysical Research Letters, 45*(6), 2826–2832.

Burrows, J. P., Weber, M., Buchwitz, M., Rozanov, V., Ladstätter-Weißenmayer, A., Richter, A., DeBeek, R., Hoogen, R., Bramstedt, K., & Eichmann, K.-U. (1999). The global ozone monitoring experiment (GOME): Mission concept and first scientific results. *Journal of the Atmospheric Sciences, 56*(2), 151–175.

Çömert, R., MATCI, D. K., & Avdan, U. (2019). Object based burned area mapping with random forest algorithm. *International Journal of Engineering and Geosciences, 4*(2), 78–87.

Elshorbany, Y. F., Kapper, H. C., Ziemke, J. R., & Parr, S. A. (2021). The status of air quality in the united states during the COVID-19 pandemic: A remote sensing perspective. *Remote Sensing, 13*(3), 369.

ESA. (2020). Sentinel-5P TROPOMI. Retrieved 18/11/2020, 2020, from https://sentinel.esa.int/web/sentinel/user-guides/sentinel-5p-tropomi

Fan, C., Li, Y., Guang, J., Li, Z., Elnashar, A., Allam, M., & de Leeuw, G. (2020). The impact of the control measures during the COVID-19 outbreak on air pollution in China. *Remote Sensing, 12*(10), 1613.

Gao, L., Wang, X., Johnson, B. A., Tian, Q., Wang, Y., Verrelst, J., Mu, X., & Gu, X. (2020). Remote sensing algorithms for estimation of fractional vegetation cover using pure vegetation index values: A review. *ISPRS Journal of Photogrammetry and Remote Sensing, 159*, 364–377.

Garane, K., Koukouli M.-E., Verhoelst T., Fioletov V., Lerot C., Heue K.-P., Bais A., Balis D., Bazureau A., & Dehn A. (2019). TROPOMI/S5ptotal ozone column data: Global ground-based validation & consistency with other satellite missions.

Ghahremanloo, M., Lops, Y., Choi, Y., & Mousavinezhad, S. (2021). Impact of the COVID-19 outbreak on air pollution levels in East Asia. *Science of the Total Environment, 754*, 142226.

Ghasempour, F., Sekertekin, A., & Kutoglu, S. H. (2021). Google Earth Engine based spatio-temporal analysis of air pollutants before and during the first wave COVID-19 outbreak over Turkey via remote sensing. *Journal of Cleaner Production, 319*, 128599.

Gopalakrishnan, V., Hirabayashi, S., Ziv, G., & Bakshi, B. R. (2018). Air quality and human health impacts of grasslands and shrublands in the United States. *Atmospheric Environment, 182*, 193–199.

Hou, Y., Wang, L., Zhou, Y., Wang, S., Liu, W., & Zhu, J. (2019). Analysis of the tropospheric column nitrogen dioxide over China based on satellite observations during 2008–2017. *Atmospheric Pollution Research, 10*(2), 651–655.

Jabeen, Z., & Khokhar, M. F. (2019). Extended database of SO2 column densities over Pakistan by exploiting satellite observations. *Atmospheric Pollution Research, 10*(3), 997–1003.

Janssen, S., Dumont, G., Fierens, F., & Mensink, C. (2008). Spatial interpolation of air pollution measurements using CORINE land cover data. *Atmospheric Environment, 42*(20), 4884–4903.

Kafy, A.-A., Rahman, M. S., Hasan, M. M., & Islam, M. (2020). Modelling future land use land cover changes and their impacts on land surface temperatures in Rajshahi, Bangladesh. *Remote Sensing Applications: Society and Environment, 18*, 100314.

Kahyaoğlu-Koračin, J., Bassett, S. D., Mouat, D. A., & Gertler, A. W. (2009). Application of a scenario-based modeling system to evaluate the air quality impacts of future growth. *Atmospheric Environment, 43*(5), 1021–1028.

Kalnay, E., Kanamitsu, M., Kistler, R., Collins, W., Deaven, D., Gandin, L., Iredell, M., Saha, S., White, G., & Woollen, J. (1996). The NCEP/NCAR 40-year reanalysis project. *Bulletin of the American Meteorological Society, 77*(3), 437–472.

Kaplan, G., & Avdan, Z. Y. (2020a). COVID-19: Spaceborne nitrogen dioxide over Turkey. *Eskişehir Technical University Journal of Science and Technology A-Applied Sciences and Engineering, 21*(2), 251–255.

Kaplan, G., & Avdan, Z. Y. (2020b). Space-borne air pollution observation from sentinel-5p tropomi: Relationship between pollutants, geographical and demographic data. *International Journal of Engineering and Geosciences, 5*(3), 130–137.

Kaplan, G., Avdan Z. Y., & Avdan U. (2019). Spaceborne Nitrogen Dioxide Observations from the Sentinel-5P TROPOMI over Turkey. Multidisciplinary Digital Publishing Institute Proceedings.

Khorrami, B., Gunduz, O., Patel, N., Ghouzlane, S., & M. NAJJAR,. (2019). Land surface temperature anomalies in response to changes in forest cover. *International Journal of Engineering and Geosciences, 4*(3), 149–156.

Metya, A., Dagupta, P., Halder, S., Chakraborty, S., & Tiwari, Y. K. (2020). COVID-19 lockdowns improve air quality in the South-East Asian regions, as seen by the remote sensing satellites. *Aerosol and Air Quality Research, 20*(8), 1772–1782.

Nacef, L., Bachari, N. E. I., Bouda, A., & Boubnia, R. (2016). Variability and decadal evolution of temperature and salinity in the mediterranean sea surface. *International Journal of Engineering and Geosciences, 1*(1), 20–29.

Ocak, S., & Turalioglu, F. S. (2008). Effect of meteorology on the atmospheric concentrations of traffic-related pollutants in Erzurum, Turkey. *J. Int. Environmental Application & Science, 3*(5), 325–335.

Oner, E., & Kaynak, B. (2016). Evaluation of NOx emissions for Turkey using satellite and ground-based observations. *Atmospheric Pollution Research, 7*(3), 419–430.

Organization, W. H. (2021). WHO global air quality guidelines: Particulate matter (PM2. 5 and PM10), ozone, nitrogen dioxide, sulfur dioxide and carbon monoxide.

Pintarić, S., Zeljković, I., Bodrožić-Džakić, T., Vrsalović, M., Zekanović, D., & Pintarić, H. (2012). Correlation between atmospheric air pollution by nitrogen dioxide meteorological parameters and the number of patients admitted to the Emergency Department. *Medica Jadertina, 42*(3–4), 97–98.

Qiu, Z., Ali, M., Nichol, J. E., Bilal, M., Tiwari, P., Habtemicheal, B. A., Almazroui, M., Mondal, S. K., Mazhar, U., & Wang, Y. (2021). Spatiotemporal investigations of multi-sensor air pollution data over Bangladesh during COVID-19 lockdown. *Remote Sensing, 13*(5), 877.

Sulla-Menashe, D., & Friedl M. A. (2018). User guide to collection 6 MODIS land cover (MCD12Q1 and MCD12C1) product. USGS: Reston, VA, USA: 1–18.

Superczynski, S. D., & Christopher, S. A. (2011). Exploring land use and land cover effects on air quality in Central Alabama using GIS and remote sensing. *Remote Sensing, 3*(12), 2552–2567.

Tadese, M., Kumar, L., Koech, R., & Kogo, B. K. (2020). Mapping of land-use/land-cover changes and its dynamics in Awash River Basin using remote sensing and GIS. *Remote Sensing Applications: Society and Environment, 19*, 100352.

Theys, N., Hedelt, P., De Smedt, I., Lerot, C., Yu, H., Vlietinck, J., Pedergnana, M., Arellano, S., Galle, B., & Fernandez, D. (2019). Global monitoring of volcanic SO 2 degassing with unprecedented resolution from TROPOMI onboard Sentinel-5 Precursor. *Scientific Reports, 9*(1), 2643.

Tobías, A., Carnerero, C., Reche, C., Massagué, J., Via, M., Minguillón, M. C., Alastuey, A., & Querol, X. (2020). Changes in air quality during the lockdown in Barcelona (Spain) one month into the SARS-CoV-2 epidemic. *Science of the Total Environment, 726*, 138540.

Ustaoglu, E., & Aydınoglu, A. C. (2019). Regional variations of land-use development and land-use/cover change dynamics: A case study of Turkey. *Remote Sensing, 11*(7), 885.

Varol, G., Tokuc, B., Ozkaya, S., & Çağlayan, Ç. (2021). Air quality and preventable deaths in Tekirdağ, Turkey. *Air Quality, Atmosphere & Health, 14*(6), 843–853.

Zhang, H., Wang, Y., Hu, J., Ying, Q., & Hu, X.-M. (2015). Relationships between meteorological parameters and criteria air pollutants in three megacities in China. *Environmental Research, 140*, 242–254.